Eigenstructure-based coherence computations as an aid to 3-D structural and stratigraphic mapping

Adam Gersztenkorn* and Kurt J. Marfurt‡

ABSTRACT

Coherence measures applied to 3-D seismic data volumes have proven to be an effective method for imaging geological discontinuities such as faults and stratigraphic features. By removing the seismic wavelet from the data, seismic coherence offers interpreters a different perspective, often exposing subtle features not readily apparent in the seismic data. Several formulations exist for obtaining coherence estimates. The first three generations of coherence algorithms at Amoco are based, respectively, on cross correlation, semblance, and an eigendecomposition of the data covariance matrix. Application of these three generations to data from the Gulf of Mexico indicates that the implementation of the eigenstructure approach described in this paper produces the most robust results. This paper first introduces the basic eigenstructure approach for computing coherence followed by a comparison on data from the Gulf of Mexico. Next, Appendix A develops a theoretical connection between the well-known semblance and the less well-known eigenstructure measures of coherence in terms of the eigenvalues of the data covariance matrix. Appendix B further extends the analysis by comparing the semblance- and eigenstructure-based coherence measures in the presence of additive uncorrelated noise.

INTRODUCTION

Measures of coherence have been used in the past in a number of applications. In particular, Taner and Koehler (1969) used semblance to compute velocity spectra by maximizing the semblance along a suite of moveout curves. Kirlin (1992) introduced an eigenstructure approach for the same application, also comparing it with the semblance approach. More recently, various coherence measures have gained popularity in 3-D structural and stratigraphic mapping. It is in this context that the following discussion proceeds.

The first generation coherence algorithm (Bahorich and Farmer, 1995, 1996), cross correlates each trace with its in-line and cross-line neighbor and then combines the two results after normalizing by the energy. Since this approach deals with only three traces, it is computationally very efficient but may lack robustness, especially when dealing with noisy data. The second generation coherence algorithm (Marfurt et al., 1998) uses a multitrace semblance measure. Using more traces in the coherence computations results in greater stability in the presence of noise. The third generation algorithm, which is presented in this paper, is also a multitrace coherence measure. However, it is based on the eigenstructure of the covariance matrix formed from the traces in the analysis cube (Gersztenkorn, 1996; Gersztenkorn and Marfurt, 1996a,b; Gersztenkorn et al., 1999). In addition, the eigenstructure algorithm incorporates various filters and interpolation schemes to aid with problems such as poor signal to noise and aliasing. These enhancements can often significantly improve the results.

A theoretical comparison of the basic semblance- and eigenstructure-based coherence estimates is discussed in the appendices. In Appendix A, it is shown that the semblance and eigenstructure coherence estimates may be compared in terms of the eigenvalues of the covariance matrix. In terms of the eigenvectors of the data covariance matrix, the semblance measure projects onto both the signal and noise subspaces, whereas the eigenstructure measure, which is a subspace approach, projects only onto the signal subspace. A subspace approach uses the eigendecomposition of the data covariance matrix to partition data in terms of signal and noise subspaces. Appendix B extends the analysis by comparing the two coherence estimates in the presence of uncorrelated noise. In this simple situation, the effect of the noise may be expressed analytically in the resulting coherence estimates.

THE EIGENSTRUCTURE COHERENCE ALGORITHM

Coherence is a mathematical measure of similarity. When applied to seismic data, coherence gives an indication of the continuity between two or more windowed seismic traces. Ideally, the degree of seismic continuity is a direct indication of geological continuity. Assigning a coherence measure on a scale of zero to one allows the seismic continuity to be quantified and translated into a visual image that reveals subtle geological features such as faults and channels. Coherence, when used for the delineation of geological features, has been applied most successfully to 3-D (time or depth) migrated seismic data. Typically, the input to the coherence algorithm is a 3-D seismic volume, resulting in the output of a corresponding 3-D coherence volume. If coherence is computed only along a horizon of interest within the 3-D seismic volume, the output coherence is one sample thick, giving rise to a coherence map.

For the computation of coherence, a 3-D analysis cube enclosing a relatively small subvolume of traces is selected by the interpreter. The analysis cube moves throughout the 3-D seismic volume and outputs a measure of coherence at each sample. The size and shape of the analysis cube defines the geometrical distribution of traces and samples to be used for the coherence computation. For the following discussion, the assumption is made that the analysis cube is a 3-D box, enclosing J traces (e.g., 3 in-line traces by 3 cross-line traces for a total of 9 traces) and N samples. Ordering each amplitude in this suite of traces by sample index n and trace index j results in the data matrix $\mathbf{D}$:

$$
\mathbf{D} = \begin{bmatrix} d_{11} & d_{12} & \cdots & d_{1J} \\ d_{21} & d_{22} & \cdots & d_{2J} \\ \vdots & \vdots & \ddots & \vdots \\ d_{N1} & d_{N2} & \cdots & d_{NJ} \end{bmatrix}. \tag{1}
$$

The matrix $\mathbf{D}$ in equation (1), which represents a multichannel time series, is a mathematical description of the data enclosed by the analysis cube. In this representation of the data, a single column of $\mathbf{D}$ represents the N samples of a single trace j, whereas a single row of $\mathbf{D}$ denotes the same time sample n, common to all J traces. The single entry d_{nj} is therefore the amplitude of the nth sample of the jth trace.

The number of samples per trace in the analysis cube is usually determined by the type of geological feature that is of interest to the interpreter. Geological features of shorter vertical duration are analyzed with smaller vertical windows; features having a longer vertical duration are analyzed with larger vertical windows. Structural features, such as faults, characterized by reflector offset often require longer windows. Stratigraphic features, such as channels, characterized by waveform tuning are better resolved with shorter windows.

The nth row of the matrix $\mathbf{D}$ is $\mathbf{d}_n^T = [d_{n1} \ d_{n2} \ \cdots \ d_{nJ}]$, and represents the value of the nth sample of each seismic trace within the analysis cube. Assuming each windowed trace has a zero mean, the sample covariance matrix for sample n is formed by the outer product:

$$
\mathbf{d}_n \mathbf{d}_n^T = \begin{bmatrix} d_{n1} \\ d_{n2} \\ \vdots \\ d_{nJ} \end{bmatrix} \begin{bmatrix} d_{n1} & d_{n2} & \cdots & d_{nJ} \end{bmatrix}
$$

$$
= \begin{bmatrix} d_{n1}^2 & d_{n1}d_{n2} & \cdots & d_{n1}d_{nJ} \\ d_{n1}d_{n2} & d_{n2}^2 & \cdots & d_{n2}d_{nJ} \\ \vdots & \vdots & \ddots & \vdots \\ d_{n1}d_{nJ} & d_{n2}d_{nJ} & \cdots & d_{nJ}^2 \end{bmatrix}. \tag{2}
$$

If the vector $\mathbf{d}_n$ is not a zero vector, then each sample covariance matrix $\mathbf{d}_n \mathbf{d}_n^T (n = 1, 2, \ldots, N)$ as represented by equation (2) is a symmetric positive semidefinite rank-one matrix. In infinite precision arithmetic, $\mathbf{d}_n \mathbf{d}_n^T$ has only one nonzero positive eigenvalue. In contrast, the full data covariance matrix $\mathbf{D}^T \mathbf{D}$, which is a sum of N rank-one matrices (from N time samples) is at most rank N or J, whichever is less, since $\mathbf{D}^T \mathbf{D}$ is a J by J matrix:

$$
\mathbf{C} = \mathbf{D}^T \mathbf{D} = \sum_{n=1}^{N} \mathbf{d}_n \mathbf{d}_n^T
$$

$$
= \begin{bmatrix} \sum_{n=1}^{N} d_{n1}^2 & \sum_{n=1}^{N} d_{n1}d_{n2} & \cdots & \sum_{n=1}^{N} d_{n1}d_{nJ} \\ \sum_{n=1}^{N} d_{n1}d_{n2} & \sum_{n=1}^{N} d_{n2}^2 & \cdots & \sum_{n=1}^{N} d_{n2}d_{nJ} \\ \vdots & \vdots & \ddots & \vdots \\ \sum_{n=1}^{N} d_{n1}d_{nJ} & \sum_{n=1}^{N} d_{n2}d_{nJ} & \cdots & \sum_{n=1}^{N} d_{nJ}^2 \end{bmatrix}. \tag{3}
$$

The rank of the matrix $\mathbf{C}$ in equation (3) is also determined, in exact arithmetic, by the number of positive eigenvalues. The number and relative size of the eigenvalues from the covariance matrix $\mathbf{C}$ determine how many degrees of freedom are present in the seismic data enclosed by the analysis cube. The eigenvalues thus give a quantitative indication of the variability present in the data.

As an example, consider a flat reflection event where all traces are identical, so that the amplitude at a given sample number is constant across all traces. This implies that the amplitude at any sample for all traces may be expressed as a scaled version of some selected single sample with amplitude not equal to zero. Without loss of generality, assume that each trace at various samples is represented in terms of the first sample. The first sample for all traces in the analysis cube is given by the first row of the matrix $\mathbf{D}$ and is $\mathbf{d}_1^T = [a \ a \ \cdots \ a]$. Under the assumption that the constant $a \neq 0$, the nth row of the matrix $\mathbf{D}$, corresponding to the nth sample of all traces, is then just a scaled version of the first sample. In this case, the nth row of the matrix $\mathbf{D}$ is $\mathbf{d}_n^T = \alpha_n \mathbf{d}_1^T = \alpha_n[a \ a \ \cdots \ a]$, and the scalar α_n is just the ratio between the nth and first sample. Forming the outer product from this newly formed vector $\mathbf{d}_n$ also results

in a rank-one matrix:

$$\mathbf{d}_n \mathbf{d}_n^T = (\alpha_n \mathbf{d}_1)(\alpha_n \mathbf{d}_1^T) = \alpha_n^2 \mathbf{d}_1 \mathbf{d}_1^T. \tag{4}$$

From equation (4), a sequence of outer-product, rank-one matrices is produced for all samples in terms of the first sample:

$$
\begin{aligned}
\mathbf{d}_1 \mathbf{d}_1^T &= \mathbf{d}_1 \mathbf{d}_1^T \\
\mathbf{d}_2 \mathbf{d}_2^T &= \alpha_2^2 \mathbf{d}_1 \mathbf{d}_1^T \\
&\vdots \\
\mathbf{d}_N \mathbf{d}_N^T &= \alpha_N^2 \mathbf{d}_1 \mathbf{d}_1^T.
\end{aligned}
\tag{5}
$$

Summation of the N rank-one, outer-product matrices in equation (5) results in the data covariance matrix $\mathbf{C}$:

$$\mathbf{C} = \mathbf{D}^T \mathbf{D} = \sum_{n=1}^{N} \mathbf{d}_n \mathbf{d}_n^T = (1 + \alpha_2^2 + \cdots + \alpha_N^2) \mathbf{d}_1 \mathbf{d}_1^T. \tag{6}$$

Since the matrix formed from the outer product $\mathbf{d}_1 \mathbf{d}_1^T$ in equation (6) is a rank-one matrix and the sum $(1 + \alpha_2^2 + \cdots + \alpha_N^2)$ is a scalar, then $\mathbf{C}$ must also be a rank-one matrix with a single positive eigenvalue. Shortly, we will demonstrate that when the traces are identical, a maximum coherence of one is achieved. In this simple situation, the high coherence value reflects the seismic continuity. As the seismic traces within the analysis cube depart from being identical, the seismic continuity and associated coherence are reduced. In general, the close proximity of the traces within the analysis cube often results in a high degree of continuity and a high associated coherence.

The covariance matrix $\mathbf{C} = \mathbf{D}^T \mathbf{D}$ in equation (3) is a symmetric positive semidefinite matrix with all eigenvalues greater than or equal to zero. A definition of the eigenstructure-based coherence estimate makes use of the numerical trace of the covariance matrix $\mathbf{C}$, denoted by $Tr(\mathbf{C})$ (Golub and Van Loan, 1989). The numerical trace of $\mathbf{C}$ may be expressed in terms of either the matrix $\mathbf{D}$, the matrix $\mathbf{C}$, or the eigenvalues of $\mathbf{C}$:

$$Tr(\mathbf{C}) = \sum_{j=1}^{J} \sum_{n=1}^{N} d_{nj}^2 = \sum_{j=1}^{J} c_{jj} = \sum_{j=1}^{J} \lambda_j. \tag{7}$$

Equation (7) demonstrates that the total energy for the traces enclosed by the analysis cube is $Tr(\mathbf{C}) \geq 0$, and is equal to the sum of the eigenvalues. The two different expressions for $Tr(\mathbf{C})$ in equation (7) may now be used for alternate definitions of the eigenstructure coherence estimate (E_c):

$$E_c = \frac{\lambda_1}{Tr(\mathbf{C})} = \frac{\lambda_1}{\sum_{j=1}^{J} c_{jj}} = \frac{\lambda_1}{\sum_{j=1}^{J} \lambda_j}, \tag{8}$$

where λ_1 is the largest eigenvalue of λ_j.

Equation (8) defines the eigenstructure coherence as a ratio of the dominant eigenvalue λ_1 to the total energy within the analysis cube. The difference in the two expressions for $Tr(\mathbf{C})$ in equation (8) can have a significant impact on the computational efficiency of the coherence calculations for 3-D seismic volumes. Summing the diagonal entries of the covariance matrix $\mathbf{C}$ is much more efficient than computing all the eigenvalues and then summing.

From equation (8), it now becomes apparent why the coherence is unity when the covariance matrix $\mathbf{C}$ is a rank-one matrix as in equation (6). Since $\mathbf{C}$ has a single nonzero eigenvalue λ_1, the expression for E_c is simply

$$E_c = \frac{\lambda_1}{\sum_{j=1}^{J} \lambda_j} = \frac{\lambda_1}{\lambda_1} = 1. \tag{9}$$

As the redundancy of the seismic data within the analysis cube is reduced, the energy becomes distributed among the other eigenvalues. Consequently, the denominator in equation (9) becomes larger than the numerator, and the coherence is diminished to a value of less than one.

Although the appendices compare the basic semblance- and eigenstructure-based coherence estimates, the eigenstructure algorithm used for the following data examples was an enhanced algorithm that was later simplified for ease of use. This enhanced algorithm has several features that produced better results, as observed in the data examples. First, within the moving analysis cube, a frequency domain filter was applied in the time/depth direction. This filter allowed the exploitation of select frequencies for their information content, as well as the avoidance of frequencies with an undesirable noise component. In addition, an alpha-trimmed mean filter (Gersztenkorn and Scales, 1988) was used between traces in the spatial direction to improve the signal-to-noise ratio. Spatial interpolation was also included to accommodate data with different record and trace spacing as well as to deal with spatial aliasing.

DATA EXAMPLES

The examples that follow (seismic data courtesy of Geco Prakla) are from the South Marsh Island area of the Gulf of Mexico, located on the continental shelf, west of and adjacent to the modern Mississippi Delta. The stacked data were time migrated, and then decimated in both time and space. The resulting volume has a sample interval of 8 ms and a trace spacing of 25 m in the in-line direction and 50 m in cross-line directions. A small subvolume with an in-line distance of 21.875 km and a cross-line distance of 14.5 km (total area of 317.1875 km²) is displayed in the following examples. The vertical cross sections in the figures are 400 ms in duration. For the coherence computations, all three generations used a time window of approximately 64 ms.

Figures 1a and 1b show two time slices at 952 ms and 1072 ms, respectively. The white lines in the two time slices indicate locations where four vertical cross-sections are extracted from both the seismic data (displayed in Figure 2) and the computed eigenstructure coherence data (displayed in Figure 3). The three coherence algorithms are displayed for comparison in Figures 4–6. Figures 4a and 4b display the eigenstructure-based coherence slices at 952 ms and 1072 ms, respectively. The cross correlation–based coherence estimate for the same two time slices is shown in Figures 5a and 5b. Figures 6a and 6b show the results of the semblance-based coherence algorithm. The coherence values are mapped to shades of gray; the darker shades indicate a lower coherence and lighter shades a higher coherence. With this convention, discontinuities such as faults appear as dark linear features.

A comparison of coherence images in cross-section with those in plan view indicates that the plan view images are more useful for detecting and interpreting geology. Visual inspection of these two views suggests a greater diversity of quality in the cross-section coherence. The subvolume under consideration contains both structural and stratigraphic features such as faults and channels. Some of the more obvious features, such as major faults, may be observed directly on the seismic cross-section (labeled as A-A′ in Figure 2a). These faults are also easily identified on the coherence slice at a time of 1072 ms in Figure 4b. In the upper portion (above 1072 ms) of the cross-section in Figure 2a, a random pattern is also present, interpreted to be the western portion of a submarine canyon. The location of this pattern may also be observed in plan view on the coherence slice in Figure 4a, where it appears as part of a large lobe of low coherence. This lobe of low coherence has been interpreted to be part of a submarine canyon.

The vertical cross section B-B′ in Figure 2b runs along the western part of the salt dome and through the center of the submarine canyon, which is seen to extend deeper within the seismic section. The random pattern filling the canyon is once more observed. Although the lobed shape of the submarine canyon is easily distinguished on the coherence slice in Figure 4a, it is not as apparent on the time slice in Figure 1a.

In Figure 4a are seen several small oblong shapes of high coherence surrounded by vast areas of lower coherence. These blocks are also identified on the vertical cross section B-B′ and the time slice in Figure 1a. Interpretation has determined that these blocks have broken away from the canyon edge while keeping their structural integrity, and through the ages have migrated toward the center of the canyon.

The vertical cross-section C-C′ in Figure 2c is located on the eastern part of the salt dome and the canyon. This cross-section contains a difficult to interpret channel that is easily identified
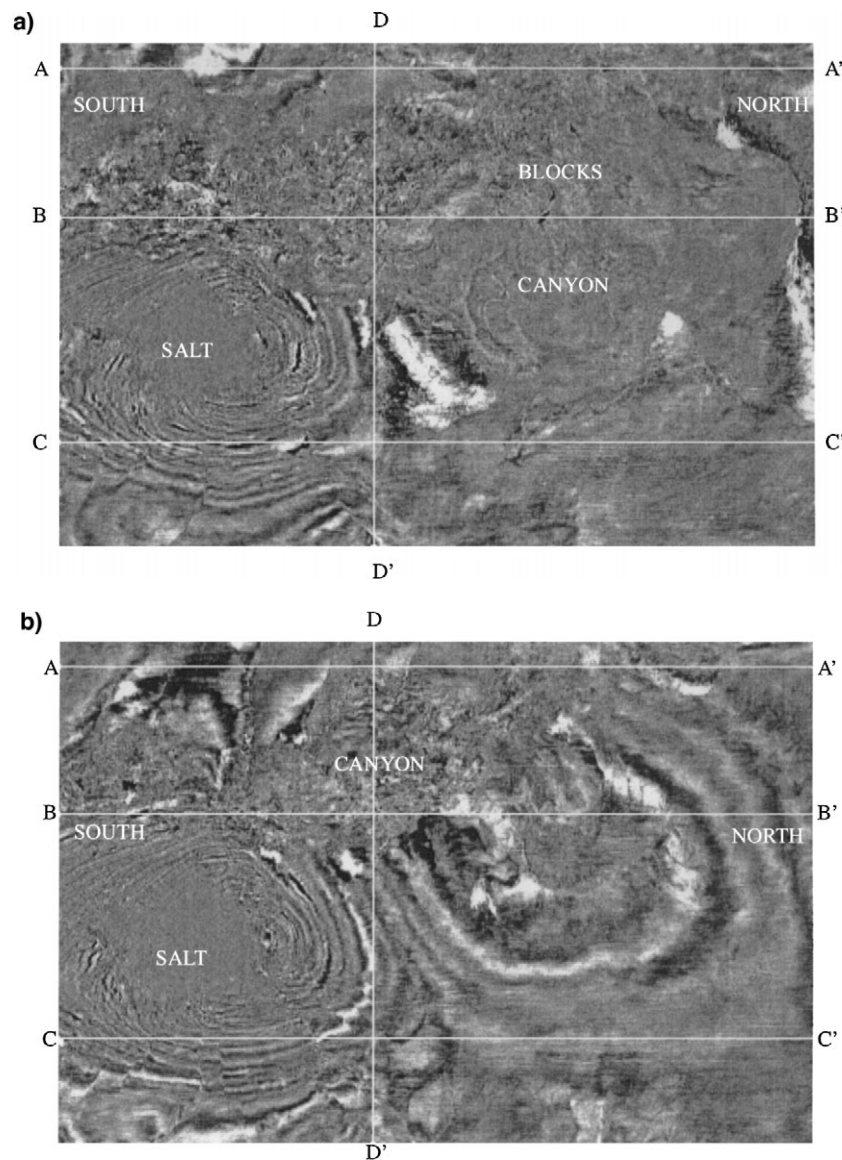

FIG. 1. Two time slices through 3-D amplitude subvolume at (a) 952 ms and (b) 1072 ms. The white lines indicate cross-sections displayed in Figures 2 and 3.
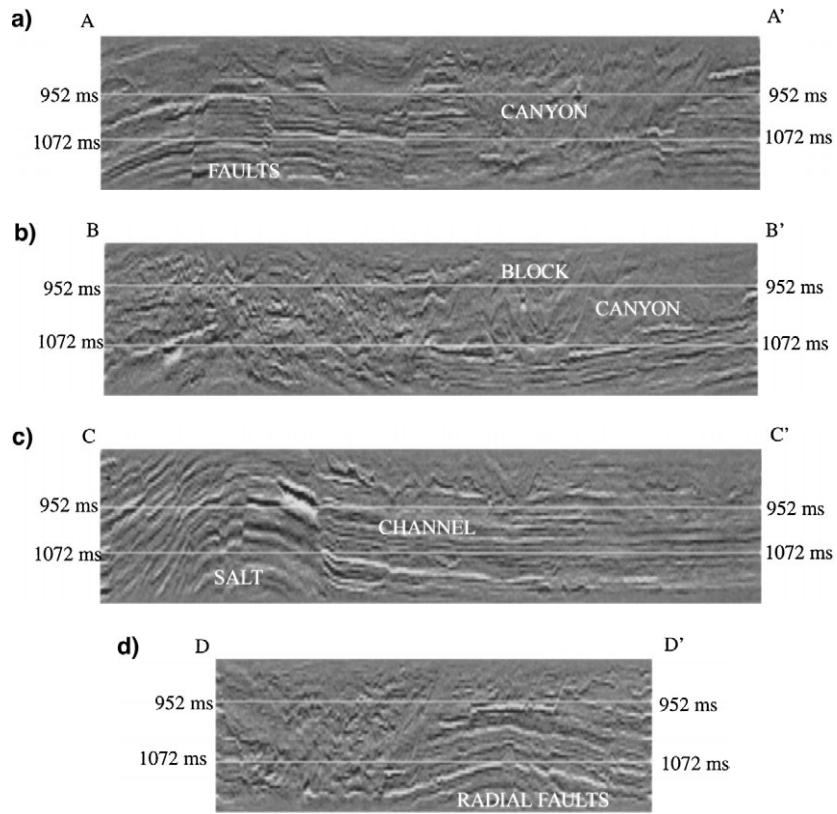
FIG. 2. Four vertical cross-sections extracted from 3-D subvolume; (a) A-A′ displaying major faults, (b) B-B′ through the center of the canyon, (c) C-C′ with channels, and (d) D-D′ through radial faults.
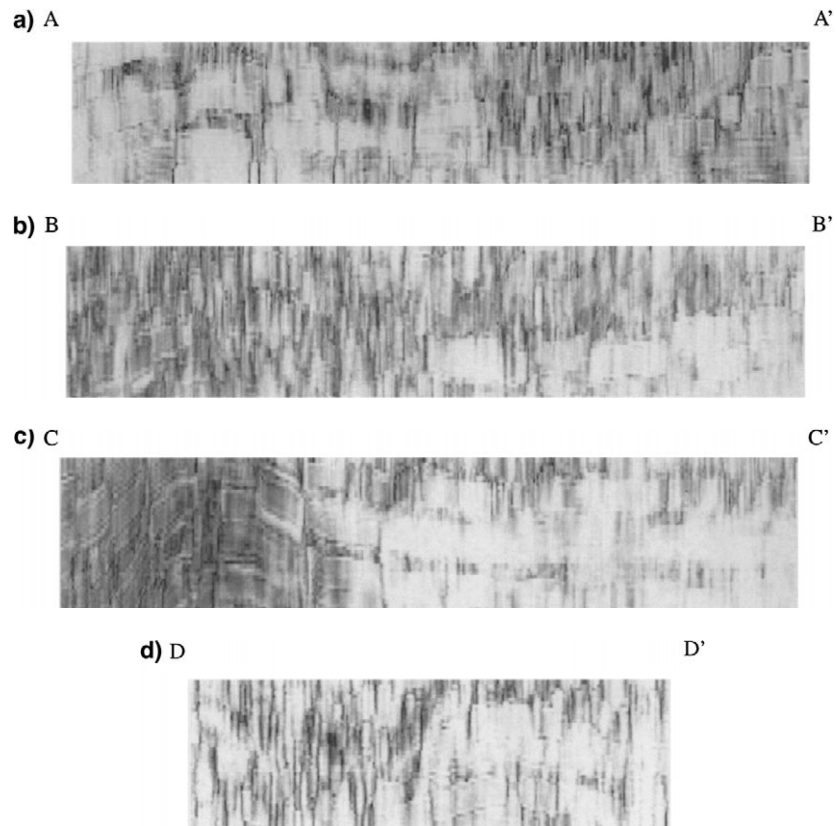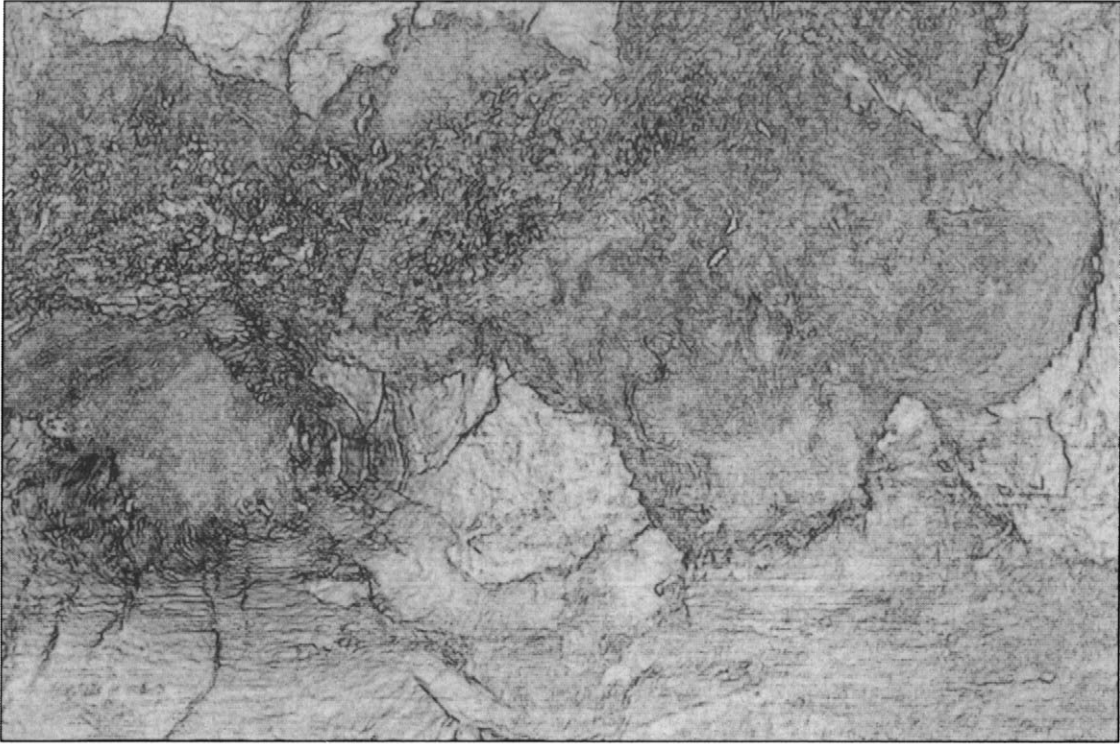

FIG. 3. Four vertical cross sections extracted from 3-D coherence subvolume corresponding to cross-sections in Figure 2.

a) SOUTH   NORTH
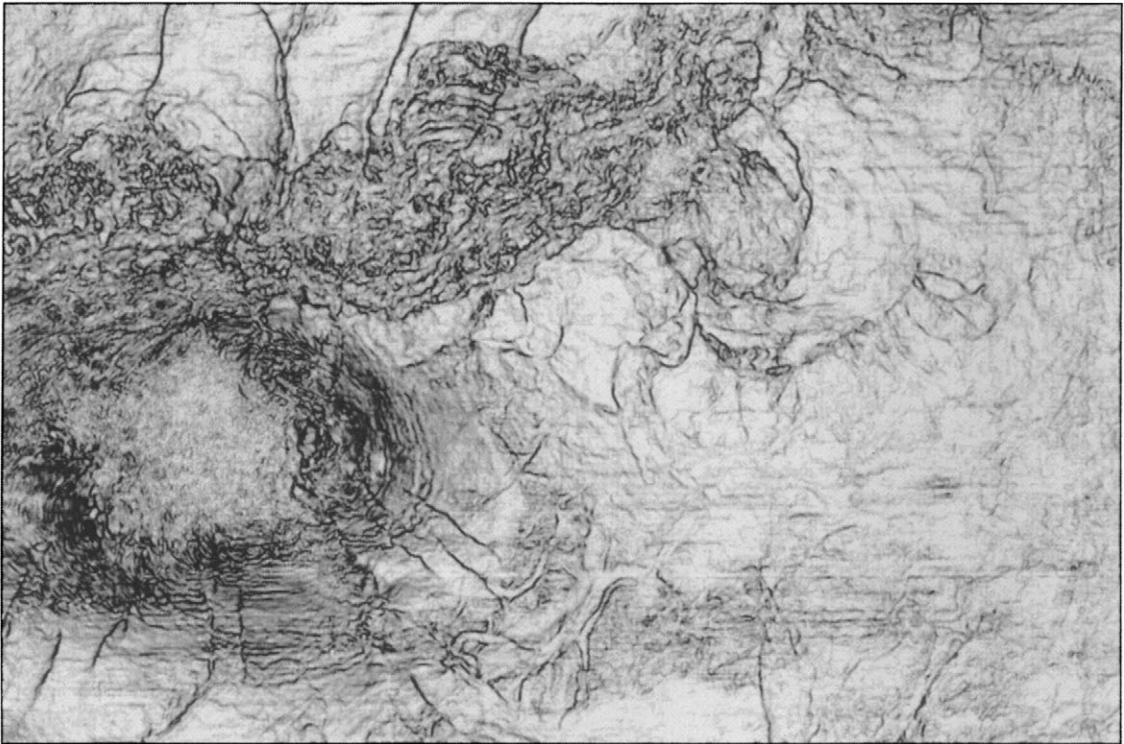

b)

FIG. 4. Two time slices through the eigenstructure-based coherence volume at (a) 952 ms and (b) 1072 ms. Note the difference between these coherence slices and the conventional amplitude slices in Figure 1.

a) SOUTH

NORTH

b)

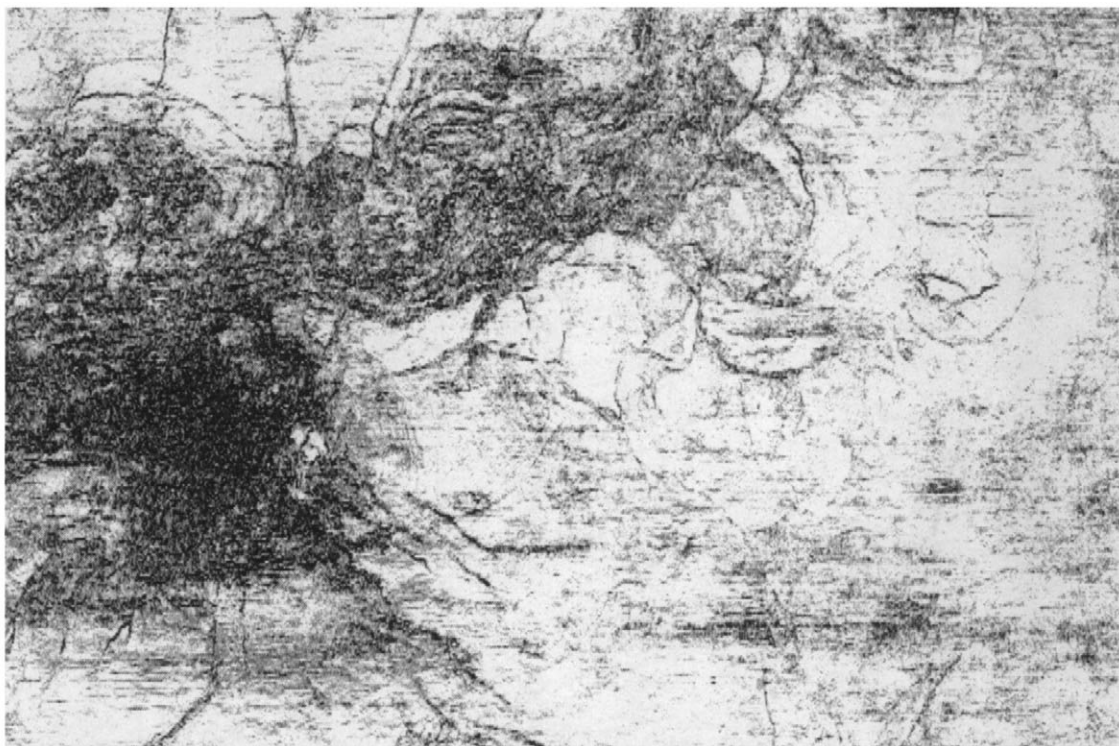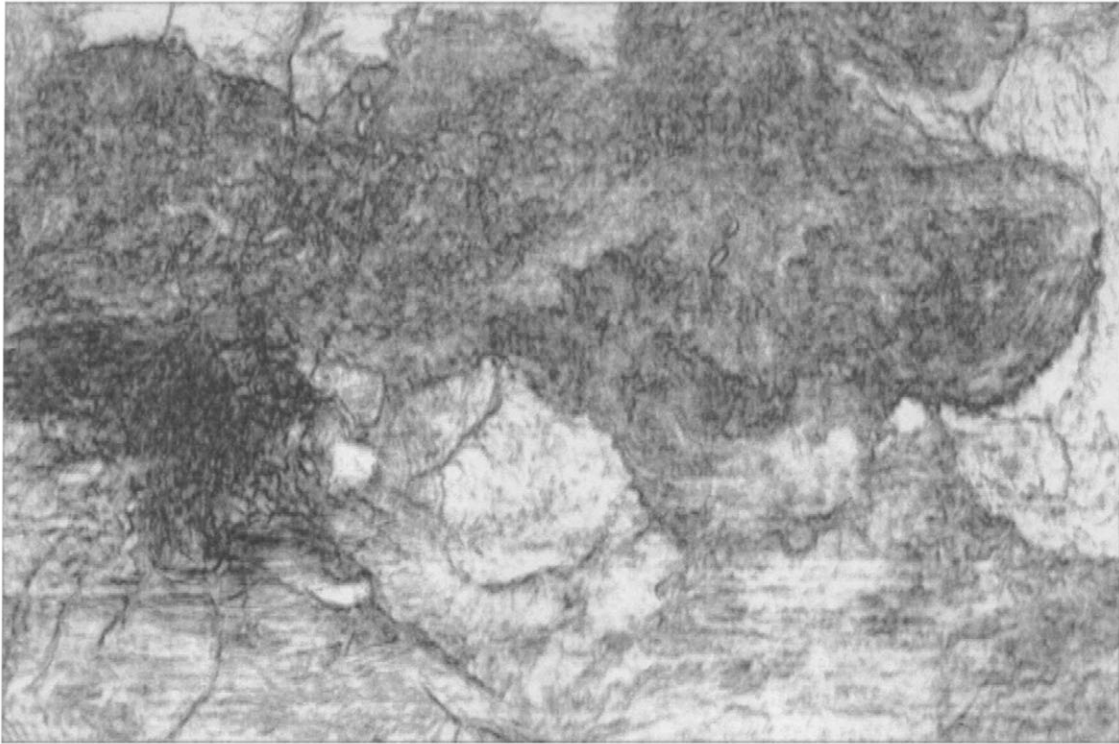FIG. 5. Two time slices through the cross correlation–based coherence volume at (a) 952 ms and (b) 1072 ms.

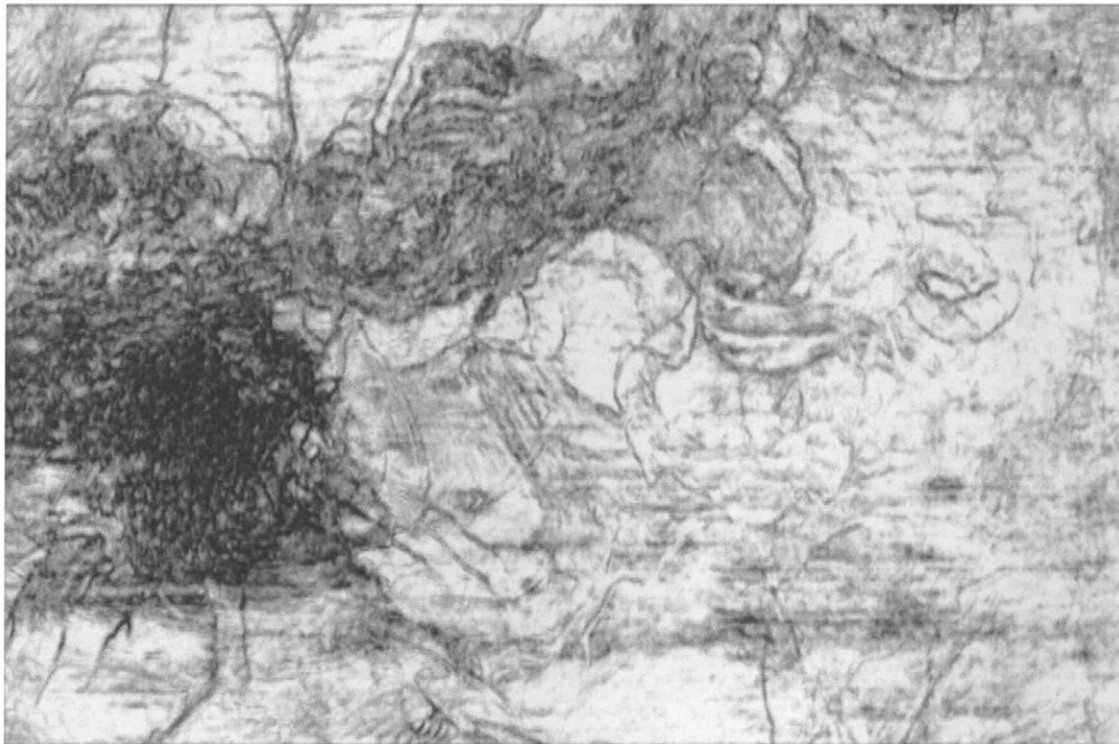a) SOUTH   NORTH

b)

FIG. 6. Two time slices through the semblance-based coherence volume at (a) 952 ms and(b) 1072 ms.

on the coherence slice in Figure 4b. Finally, Figure 2d displays cross section D-D′ on the northern part of the salt dome. The radial faults in close proximity to the salt dome are not easily distinguished on the cross-section in Figure 2c or the time slice in Figure 1b (both at 1072 ms). The coherence slice, on the other hand, clearly reveals the two radial faults protruding from the salt dome. For more details on the interpretation of this data, see Nissen et al. (1995).

CONCLUSION

Three-dimensional seismology is becoming an increasingly important exploration tool by providing a detailed structural and stratigraphic image of the subsurface. Seismic coherence techniques have further contributed to the use of 3-D seismic by allowing interpreters to visualize geology from a data-oriented perspective which is not directly dependent on the seismic data. This can often produce a more natural setting for interpreters to visualize geological processes.

In this paper, the eigenstructure-based coherence algorithm has been formulated and applied to the detection and imaging of geological discontinuities. In Appendix A, the semblance-based coherence algorithm is analyzed in terms of the eigendecomposition of the covariance matrix, and a relationship is established with the eigenstructure coherence estimate. Appendix B describes the behavior of the semblance and eigenstructure coherence estimates in the presence of additive noise.

The data examples compare three generations of coherence algorithms on a small 3-D seismic subvolume from the Gulf of Mexico. The results indicate that the described implementation of the eigenstructure-based coherence estimate provides a more robust measure of coherence that lends itself to the detection of discontinuities in seismic data. A brief discussion also indicates how the coherence images are used to interpret the geological phenomena recorded in seismic data.

REFERENCES

Bahorich, M. S., and Farmer, S. L., 1995, 3-D seismic discontinuity for faults and stratigraphic features: The Leading Edge, **14**, 1053–1058.
———— 1999, Methods of seismic signal processing and exploration: US Patent 5 563 949.
Gersztenkorn, A., 1999, Method and apparatus for seismic signal processing and exploration: US Patent 5 892 732.
Gersztenkorn, A., and Marfurt, K. J., 1996a, Coherence computations with eigenstructure: 58th Conf. and Tech. Exhibition, Eur. Assn. Geosci. Eng., Extended Abstracts, X031.
———— 1996b, Eigenstructure based coherence computations: 66th Ann. Internat. Mtg., Soc. Expl. Geophys., Expanded Abstracts, 328–331.
Gersztenkorn, A., and Scales, J. A., 1988, Smoothing seismic tomograms with alpha-trimmed means: Geophy. J., **92**, 67–72.
Gersztenkorn, A., Sharp, J., and Marfurt, K., 1999, Delineation of tectonic features offshore Trinidad using 3-D seismic coherence: The Leading Edge, **18**, scheduled for September.
Golub, G. H., and Van Loan, C. F., 1989, Matrix computations: John Hopkins Univ. Press.
Kirlin, R. L., 1992, The relationship between semblance and eigenstructure velocity estimators: Geophysics, **57**, 1027–1033.
Marfurt, K. J., Kirlin, R. L., Farmer, S. L., and Bahorich, M. S., 1998, 3-D seismic attributes using a semblance-based coherency algorithm: Geophysics, **63**, 1150–1165.
Sheriff, R. E., 1984, Encyclopedic dictionary of exploration geophysics: Soc. Expl. Geophys.
Nissen, S. E., Haskell, N. L., Lopez, J. A., Donlon, T. J., and Bahorich, M. S, 1997, 3-D seismic coherency techniques applied to the identification and delineation of slump features: 65th Ann. Internat. Mtg., Soc. Expl. Geophys., Expanded Abstracts, 1532–1534.
Taner, M. T., and Koehler, F., 1969, Velocity spectra—Digital computer derivation and applications of velocity functions, Geophysics, **34**, 859–881.

APPENDIX A

COMPARISON OF SEMBLANCE AND EIGENSTRUCTURE COHERENCE

For a comparison of the basic semblance and eigenstructure based coherence estimates, the data covariance matrix $\mathbf{C}$ from equation (3) is expressed in terms of its eigendecomposition:

$$\mathbf{C} = \mathbf{V}\boldsymbol{\Lambda}\mathbf{V}^T. \qquad (A\text{-}1)$$

The eigenvalues of $\mathbf{C}$ in equation (A-1) are arranged in descending order in the diagonal matrix $\boldsymbol{\Lambda}$. The matrix $\mathbf{V} = [\mathbf{v}_1 \ \mathbf{v}_2 \ \cdots \ \mathbf{v}_J]$ is a J by J matrix whose columns are the eigenvectors of $\mathbf{C}$. By construction, the eigenvectors of $\mathbf{C}$ form an orthonormal set (Golub and Van Loan, 1989). The orthonormal property of the eigenvectors is next used to show that the numerator of the eigenstructure coherence estimate is expressible in terms of either the dominant eigenvalue λ_1 or the associated eigenvector $\mathbf{v}_1$. This produces two equivalent expressions for the eigenstructure-based coherence estimate:

$$E_c = \frac{\lambda_1}{Tr(\mathbf{C})} = \frac{\mathbf{v}_1^T \mathbf{C}\mathbf{v}_1}{Tr(\mathbf{C})}. \qquad (A\text{-}2)$$

Equivalence of the numerators for E_c in equation (A-2) is established by using the eigendecomposition of the matrix $\mathbf{C}$ from equation (A-1). To extract the dominant eigenvalue (λ_1), the associated eigenvector $\mathbf{v}_1$ is first distributed to the other eigenvectors. Subsequently, applying the orthonormal property of the eigenvectors achieves the desired result (Golub and Van Loan, 1989):

$$\mathbf{v}_1^T \mathbf{C}\mathbf{v}_1 = \mathbf{v}_1^T \mathbf{V}\boldsymbol{\Lambda}\mathbf{V}^T \mathbf{v}_1 = \lambda_1 \qquad (A\text{-}3)$$

Since $\mathbf{v}_1^T \mathbf{C}\mathbf{v}_1$ is equal to λ_1, the equivalence of the two expressions for E_c in equation (A-2) is established. This equivalence will be used later in this appendix.

To facilitate comparison between the semblance and eigenstructure coherence estimates, an expression for the semblance must be established in terms of the covariance matrix $\mathbf{C}$. A well-known definition for the semblance (S_c), in terms of the data

matrix $\mathbf{D}$ is defined by the summation (Sheriff, 1984):

$$S_c = \frac{\sum_{n=1}^{N}\left[\sum_{j=1}^{J} d_{nj}\right]^2}{J \sum_{n=1}^{N}\sum_{j=1}^{J}(d_{nj})^2}. \tag{A-4}$$

An alternate but equivalent expression for S_c, which is better suited for the analysis to follow, is obtained from the data covariance matrix $\mathbf{C} = \mathbf{D}^T\mathbf{D}$:

$$S_c = \frac{\mathbf{u}^T\mathbf{C}\mathbf{u}}{Tr(\mathbf{C})}. \tag{A-5}$$

The normalized vector $\mathbf{u}$ (i.e., $\|\mathbf{u}\|_2 = 1$) in equation (A-5) is used to sum the entries in the matrix $\mathbf{C}$ and is defined as

$$\mathbf{u} = \frac{1}{\sqrt{J}}\begin{bmatrix}1\\1\\\vdots\\1\end{bmatrix}. \tag{A-6}$$

Looking back, it is observed that E_c in equation (A-2) is expressed in terms of the eigenvector $\mathbf{v}_1$, whereas equa-

tion (A-5) expresses S_c by use of the normalized vector $\mathbf{u}$. To establish a connection between S_c and E_c, the normalized vector $\mathbf{u}$ is first defined in terms of the eigenvectors of the matrix $\mathbf{C}$. This is possible, since the J orthonormal eigenvectors $\mathbf{V} = [\mathbf{v}_1 \ \mathbf{v}_2 \ \cdots \ \mathbf{v}_J]$ are linearly independent and span the real J-dimensional space $\mathbf{R}^J$. Each of the individual eigenvectors $\mathbf{v}_j \in \mathbf{V}$ $(j = 1, 2, \ldots, J)$, spans a subspace of $\mathbf{R}^J$. The vector $\mathbf{u} \in \mathbf{R}^J$, used in the computation of S_c, is a J-dimensional vector and may therefore be reconstructed from a linear combination of the eigenvectors of the matrix $\mathbf{C}$:

$$\mathbf{u} = \beta_1\mathbf{v}_1 + \beta_2\mathbf{v}_2 + \cdots + \beta_J\mathbf{v}_J. \tag{A-7}$$

Taking the inner product between $\mathbf{u}$ and each eigenvector $\mathbf{v}_j$, determines the scalar weights β_j $(j = 1, 2, \ldots, J)$ that need to be assigned to each eigenvector for a reconstruction of $\mathbf{u}$ in equation (A-7). Since both $\mathbf{u}$ and $\mathbf{v}_j$ are normalized, a simple expression exists for the inner products:

$$\beta_j = \mathbf{u}^T\mathbf{v}_j = \|\mathbf{u}\|_2 \|\mathbf{v}_j\|_2 \cos\theta_j = \cos\theta_j. \tag{A-8}$$

The weights in equation (A-8) denote the amount by which the normalized vector $\mathbf{u}$ projects onto each of the eigenvectors $\mathbf{v}_j$ $(j = 1, 2, \ldots, J)$, which in turn depends on the angle between the two vectors. Using the weights from equation (A-8) allows the vector $\mathbf{u}$ to be expressed as a linear combination of the eigenvectors:

$$\mathbf{u} = \mathbf{v}_1\cos\theta_1 + \mathbf{v}_2\cos\theta_2 + \cdots + \mathbf{v}_J\cos\theta_J. \tag{A-9}$$

It is useful for the discussion in Appendix B to establish the fact that the sum of the squared weights is one (i.e., $\sum_{j=1}^{J}\beta_j^2 = \sum_{j=1}^{J}\cos^2\theta_j = 1$). This is accomplished by using the orthonormal property of the eigenvectors and the normalization of the vector $\mathbf{u}$ from equation (A-6):

$$\|\mathbf{u}\|_2^2 = \mathbf{u}^T\mathbf{u}$$

$$= (\beta_1\mathbf{v}_1 + \beta_2\mathbf{v}_2 + \cdots + \beta_J\mathbf{v}_J)^T$$

$$\times (\beta_1\mathbf{v}_1 + \beta_2\mathbf{v}_2 + \cdots + \beta_J\mathbf{v}_J) \tag{A-10}$$

$$= \sum_{j=1}^{J}\beta_j^2 = \sum_{j=1}^{J}\cos^2\theta_j = 1.$$

From equation (A-9), the difference between S_c and E_c is now starting to become more apparent. Whereas S_c uses the vector $\mathbf{u}$, which is a linear combination of all the eigenvectors, E_c uses only $\mathbf{v}_1$, the eigenvector associated with the largest eigenvalue. In other words, S_c and E_c use different subspaces for computing coherence.

The expression for $\mathbf{u}$ in equation (A-9) is now substituted directly into the expression for the semblance coherence S_c in equation (A-5):

$$S_c = \frac{\mathbf{u}^T\mathbf{C}\mathbf{u}}{Tr(\mathbf{C})} = \frac{(\beta_1\mathbf{v}_1 + \beta_2\mathbf{v}_2 + \cdots + \beta_J\mathbf{v}_J)^T\mathbf{C}(\beta_1\mathbf{v}_1 + \beta_2\mathbf{v}_2 + \cdots + \beta_J\mathbf{v}_J)}{Tr(\mathbf{C})}. \tag{A-11}$$

Multiplying all the terms, and again making use of the orthonormal property of the eigenvectors leads to a somewhat simpler expression:

$$S_c = \frac{\beta_1^2\mathbf{v}_1^T\mathbf{C}\mathbf{v}_1 + \beta_2^2\mathbf{v}_2^T\mathbf{C}\mathbf{v}_2 + \cdots + \beta_J^2\mathbf{v}_J^T\mathbf{C}\mathbf{v}_J}{Tr(\mathbf{C})}. \tag{A-12}$$

To establish equivalence of the two expressions in equation (A-2), it was shown in equation (A-3) that $\mathbf{v}_1^T\mathbf{C}\mathbf{v}_1 = \lambda_1$. A similar procedure is used for each eigenvector $\mathbf{v}_j$ to establish that $\mathbf{v}_j^T\mathbf{C}\mathbf{v}_j = \lambda_j$ $(j = 2, 3, \ldots, J)$. Replacing each term in the numerator of equation (A-12) with its eigenvalue equivalent allows the numerator of S_c to be written as a weighted sum of eigenvalues. Finally, using the relation established from equation (A-8) that $\beta_j = \cos\theta_j$ produces the desired expression for S_c:

$$S_c = \frac{\lambda_1\cos^2\theta_1 + \lambda_2\cos^2\theta_2 + \cdots + \lambda_J\cos^2\theta_J}{Tr(\mathbf{C})}. \tag{A-13}$$

It is now apparent from equation (A-13) that each weight in the numerator of S_c depends on the angle between the subspace spanned by the vector $\mathbf{u}$ and the subspace spanned by each of the eigenvectors $\mathbf{v}_j$. Each weight thus determines the contribution of the corresponding eigenvalue. In the special case where $\mathbf{u} = \mathbf{v}_1$, the angles in equation (A-13) are

$$\theta_1 = 0, \theta_2 = \theta_3 = \cdots = \theta_J = \frac{\pi}{2}. \tag{A-14}$$

The corresponding weights $\beta_j = \cos\theta_j$ associated with each angle are

$$\cos\theta_1 = 1, \cos\theta_2 = \cos\theta_3 = \cdots = \cos\theta_J = 0. \quad \text{(A-15)}$$

As one would imagine, in this case S_c and E_c are identical:

$$S_c = \frac{\lambda_1}{Tr(\mathbf{C})} = E_c. \quad \text{(A-16)}$$

In general, the vector $\mathbf{u}$ is not equal to the eigenvector $\mathbf{v}_1$. As the analysis cube moves throughout the 3-D volume, the covariance matrix $\mathbf{C}$ and associated eigenvector $\mathbf{v}_1$, which are dynamic quantities, adjust and change with each different location. In contrast, the vector $\mathbf{u}$ is static and remains constant as the analysis cube progresses through the seismic volume.

Bounds for the semblance and eigenstructure coherence estimates may be derived by the Rayleigh quotient (Golub and Van Loan, 1989). The Rayleigh quotient states that for any normalized vector $\mathbf{u}$ (i.e., $\|\mathbf{u}\|_2 = 1$) and a positive, semidefinite, J by J matrix $\mathbf{C}$, the Rayleigh quotient, defined as $\mathbf{u}^T\mathbf{C}\mathbf{u}$, satisfies the inequality

$$\lambda_1 \geq \mathbf{u}^T\mathbf{C}\mathbf{u} \geq \lambda_J, \quad \text{(A-17)}$$

where the eigenvalues λ_1 and λ_J in equation (A-17) are, respectively, the largest and smallest eigenvalues of $\mathbf{C}$. Dividing each term in equation (A-17) by $Tr(\mathbf{C})$ produces the desired inequality relationship between the semblance- and eigenstructure-based coherence estimates:

$$\frac{\lambda_1}{Tr(\mathbf{C})} \geq \frac{\mathbf{u}^T\mathbf{C}\mathbf{u}}{Tr(\mathbf{C})} \geq \frac{\lambda_J}{Tr(\mathbf{C})}. \quad \text{(A-18)}$$

Using previously defined notation, the inequality in equation (A-18) is

$$E_c \geq S_c \geq \frac{\lambda_J}{Tr(\mathbf{C})}. \quad \text{(A-19)}$$

Writing out the inequality of equation (A-19) in full detail reveals the interaction of the eigenvalues for the different coherence estimates:

$$\frac{\lambda_1}{Tr(\mathbf{C})} \geq \frac{\lambda_1\cos^2\theta_1 + \lambda_2\cos^2\theta_2 + \cdots + \lambda_J\cos^2\theta_J}{Tr(\mathbf{C})}$$
$$\geq \frac{\lambda_J}{Tr(\mathbf{C})}. \quad \text{(A-20)}$$

In equation (A-20), the comparison between S_c and E_c is complete. Each eigenvalue is used according to the projection of the normalized vector $\mathbf{u}$ onto the corresponding eigenvector. It is worth noting that often the relative size of the small eigenvalues is such that they don't contribute much to the semblance-based coherence estimate.

APPENDIX B

COHERENCE FOR SIGNALS WITH ADDITIVE UNCORRELATED NOISE

The eigenvector $\mathbf{v}_1$ defines E_c by extracting the signal subspace, which in turn is dependent on the redundancy present in seismic data. In this formalism, the subspace associated with some of the other eigenvectors is considered part of the noise subspace. In contrast, note that the vector $\mathbf{u}$ in equation (A-9) can include components from all the eigenvectors. In principle, as $\mathbf{u}$ departs from the signal subspace, the semblance coherence estimate S_c becomes increasingly more corrupted by the noise component in the data. The presence of large eigenvalues associated with the noise subspace can therefore have a detrimental effect. It is instructive to consider the effect of noise in a simple situation.

Consider the situation where the data enclosed by the analysis cube, as represented by the matrix $\mathbf{D}$, contains both a signal and a noise component. This is expressed as $\mathbf{D} = \mathbf{S} + \mathbf{N}$, where $\mathbf{D}$ is the composite matrix, and $\mathbf{S}$ and $\mathbf{N}$ are, respectively, the signal and noise matrices. As previously demonstrated in equation (3), the data covariance matrix $\mathbf{C}$ is formed by

$$\mathbf{C} = \mathbf{D}^T\mathbf{D} = (\mathbf{S} + \mathbf{N})^T(\mathbf{S} + \mathbf{N})$$
$$= \mathbf{S}^T\mathbf{S} + \mathbf{S}^T\mathbf{N} + \mathbf{N}^T\mathbf{S} + \mathbf{N}^T\mathbf{N}. \quad \text{(B-1)}$$

The first assumption made is that the noise is random and uncorrelated with the signal and with itself. This establishes the following relationships for particular terms in equation (B-1):

$$\mathbf{S}^T\mathbf{N} = \mathbf{N}^T\mathbf{S} = \mathbf{0} \quad \text{and} \quad \mathbf{N}^T\mathbf{N} = \sigma^2\mathbf{I} = \mathbf{C}_N. \quad \text{(B-2)}$$

In equation (B-2), $\mathbf{0}$ denotes the zero matrix and indicates orthogonality between signal and noise. The covariance of the noise is $\sigma^2\mathbf{I}$, where $\mathbf{I}$ is the diagonal identity matrix and σ^2 is the variance of the noise component. Using the notation $\mathbf{C}_D = \mathbf{D}^T\mathbf{D}$ and $\mathbf{C}_S = \mathbf{S}^T\mathbf{S}$ as the covariance of the data and signal, respectively, produces a compact representation of the data covariance matrix:

$$\mathbf{C}_D = \mathbf{C}_S + \sigma^2\mathbf{I}. \quad \text{(B-3)}$$

Assuming the signal covariance matrix $\mathbf{C}_S$ has the eigenpairs $(\mu_j, \mathbf{v}_j)$, then basic eigenvalue theory indicates that $\mathbf{C}_S\mathbf{v}_j = \mu_j\mathbf{v}_j$. The eigendecomposition of the signal covariance matrix $\mathbf{C}_S$ may now be related to the eigendecomposition of the data covariance matrix $\mathbf{C}_D$. This is accomplished by adding $\sigma^2\mathbf{I}\mathbf{v}_j$ to both sides of the eigendecomposition $\mathbf{C}_S\mathbf{v}_j = \mu_j\mathbf{v}_j$:

$$\mathbf{C}_S\mathbf{v}_j = \mu_j\mathbf{v}_j,$$
$$\mathbf{C}_S\mathbf{v}_j + \sigma^2\mathbf{I}\mathbf{v}_j = \mu_j\mathbf{v}_j + \sigma^2\mathbf{I}\mathbf{v}_j,$$
$$(\mathbf{C}_S + \sigma^2\mathbf{I})\mathbf{v}_j = (\mu_j + \sigma^2)\mathbf{v}_j, \quad \text{and}$$
$$\mathbf{C}_D\mathbf{v}_j = \lambda_j\mathbf{v}_j. \quad \text{(B-4)}$$

Equation (B-4) relates the eigenpairs $(\mu_j, \mathbf{v}_j)$ of the noise-free covariance matrix $\mathbf{C}_S$, to the eigenpairs $(\lambda_j, \mathbf{v}_j) = (\mu_j + \sigma^2, \mathbf{v}_j)$ belonging to the composite matrix $\mathbf{C}_D$. It is interesting to note that although the eigenvalues of $\mathbf{C}_S$ and $\mathbf{C}_D$ differ by the variance of the noise, the eigenvectors remain the same.

The next step is to assume that the signal is correlated with itself, which occurs when the covariance matrix $\mathbf{C}_S$ is

formed from identical seismic traces. This implies that the matrix $\mathbf{C}_S$ is a rank-one matrix and, as was shown earlier, has a single positive eigenvalue. The composite matrix $\mathbf{C}_D$, which contains both signal and noise components, has eigenvalues λ_j ($j = 1, 2, \ldots, J$) defined by

$$\lambda_1 = \mu_1 + \sigma^2, \text{ and}$$
$$\lambda_j = \sigma^2, \ j = 2, 3, \ldots, J. \tag{B-5}$$

For this greatly simplified situation, equation (B-5) indicates that the composite matrix $\mathbf{C}_D$ includes both signal and noise in the first eigenvalue, while only the variance of the noise is present in the last $J - 1$ eigenvalues. This suggests an obvious procedure for estimating noise in a more general setting: simply average a predetermined number of the smallest eigenvalues. When the traces are identical except for noise, averaging the last $J - 1$ eigenvalues results in a simple expression:

$$\sigma^2 = \frac{\displaystyle\sum_{j=2}^{J} \lambda_j}{J - 1} = \frac{Tr(\mathbf{C}) - \lambda_1}{J - 1}. \tag{B-6}$$

The approximation of the noise in equation (B-6) is an idealization and is statistically dependent on the number of measurements used.

The eigenvalues in equation (B-5) may now be used to form the two coherence estimates. Using the definition in equation (A-2) for E_c, results in

$$E_c = \frac{\lambda_1}{Tr(\mathbf{C}_D)} = \frac{\mu_1 + \sigma^2}{\mu_1 + J\sigma^2}. \tag{B-7}$$

As equation (B-7) illustrates, E_c is corrupted by the variance of the noise resulting in a coherence of less than one. In contrast, an expression for S_c is attained by substituting the eigenvalues of equation (B-5) into equation (A-13). Using $\cos \theta_j = \beta_j$

expresses S_c as a weighted sum of the eigenvalues:

$$S_c \frac{\displaystyle\sum_{j=1}^{J} \beta_j^2 \lambda_j}{Tr(\mathbf{C}_D)} = \frac{\beta_1^2 (\mu_1 + \sigma^2) + \displaystyle\sum_{j=2}^{J} \beta_j^2 \sigma^2}{\mu_1 + J\sigma^2}$$

$$= \frac{\beta_1^2 \mu_1 + \sigma^2 \displaystyle\sum_{j=1}^{J} \beta_j^2}{\mu_1 + J\sigma^2}. \tag{B-8}$$

Applying the results that $\sum_{j=1}^{J} \beta_j^2 = 1$ from equation (A-10) and $\beta_1^2 = \cos^2 \theta_1$ from equation (A-8) simplifies the expression for S_c in equation (B-8):

$$S_c = \frac{\mu_1 \cos^2 \theta_1 + \sigma^2}{\mu_1 + J\sigma^2}. \tag{B-9}$$

Equation (B-9) again illustrates the dependence of S_c on the angle between the signal subspace spanned by the eigenvector $\mathbf{v}_1$ and the subspace spanned by the vector $\mathbf{u}$. Since E_c uses the subspace spanned by the eigenvector $\mathbf{v}_1$, there is no such dependence. In the pathological case when the angle θ_1 goes to $\pi/2$, the weight $\cos^2 \theta_1$ goes to zero, and the eigenvalue μ_1, associated with the signal is left out of the S_c estimate entirely. In this case, the vector $\mathbf{u}$ becomes orthogonal to the signal subspace, and the numerator of S_c only picks up information from the noise subspace:

$$S_c = \frac{\sigma^2}{\mu_1 + J\sigma^2}. \tag{B-10}$$

With only uncorrelated noise in the signal, the eigenvalues of the composite matrix $\mathbf{C}_D = \mathbf{N}^T \mathbf{N} = \sigma^2 \mathbf{I}$ are equal to the variance of the noise ($\lambda_j = \sigma^2$, $j = 1, 2, \ldots, J$). Substitution of these eigenvalues into the appropriate expressions demonstrates that both the coherence estimates S_c and E_c are equal to the inverse of the number of traces in the analysis cube:

$$S_c = E_c = \frac{\sigma^2}{J\sigma^2} = \frac{1}{J}. \tag{B-11}$$